Localization switching of a large object in a crowded cavity: A rigid/soft object prefers surface/inner positioning

Chwen-Yang Shew, Soutaro Oda, and Kenichi Yoshikawa

Citation: The Journal of Chemical Physics **147**, 204901 (2017);
View online: https://doi.org/10.1063/1.5000762
View Table of Contents: http://aip.scitation.org/toc/jcp/147/20
Published by the American Institute of Physics

Localization switching of a large object in a crowded cavity: A rigid/soft object prefers surface/inner positioning

Chwen-Yang Shew,[1,a)] Soutaro Oda,[2] and Kenichi Yoshikawa[2]
[1]*Ph.D. Program in Chemistry, The Graduate Center of the City University of New York, New York, New York 10016, USA and Department of Chemistry, College of Staten Island, Staten Island, New York 10314, USA*
[2]*Faculty of Life and Medical Sciences, Doshisha University, Kyotanabe 610-0394, Japan*

(Received 18 August 2017; accepted 23 October 2017; published online 22 November 2017)

For living cells in the real world, a large organelle is commonly positioned in the inner region away from membranes, such as the nucleus of eukaryotic cells, the nucleolus of nuclei, mitochondria, chloroplast, Golgi body, etc. It contradicts the expectation by the current depletion-force theory in that the larger particle should be excluded from the inner cell space onto cell boundaries in a crowding media. Here we simply model a sizable organelle as a soft-boundary large particle allowing crowders, which are smaller hard spheres in the model, to intrude across its boundary. The results of Monte Carlo simulation indicate that the preferential location of the larger particle switches from the periphery into the inner region of the cavity by increasing its softness. An integral equation theory is further developed to account for the structural features of the model, and the theoretical predictions are found consistent with our simulation results. *Published by AIP Publishing.* https://doi.org/10.1063/1.5000762

I. INTRODUCTION

Eukaryotic cells exhibit a unique structural feature consisting of a nucleus embedded in the highly crowded cellular cytoplasm with 30%-40% of space occupied by cellular materials.[1,2] The nucleus is a large organelle that can take up around 10% of cell volume.[3,4] Traditionally it is known that for an animal cell, the nucleus distributes near the center of the cell.[5] As for a plant cell, the cellular vacuole occupies the central region of the cell due to its size though cellular activities cause some spatial fluctuation.[6,7] Besides nuclei in cells, the nucleolus in a nucleus displays a similar structure in that the nucleolus is preferentially distributed away from the peripheral region.[8] Other significantly large cellular organelles, such as mitochondria, chloroplast, Golgi body, etc., are often positioned in the inner cell region away from membranes.[9] Despite the dynamical nature of cellular matters,[7] the traditional picture suggests the existence of a statistical sense to account for the mean positioning of a large organelle in the cell.

Considering molecular crowding and electrostatic screening in cellular physiological condition, excluded volume interaction can be highly significant compared to short- and long-ranged intermolecular forces among cellular materials.[10,11] In other words, the entropic effect may play a major role rather than the enthalpic effect to elucidate intracellular structures. From the standpoint of entropy, the preferential location of the nucleus away from cellular membranes in animal cells indeed contradicts to the usual physical picture. If cells are viewed as a cavity, then the large particle should have a great tendency to localize adjacent to the cavity wall to increase the free space (or to increase entropy) for smaller particles.[12] Obviously, this depletion force picture is not applicable to interpret the fact that a nucleus is located in the region away from membranes or even near the center of a cell. Note that the depletion forces between hard sphere liquids near a spherical cavity wall are not exactly the same as those close to a flat wall, and the curvature of the spherical cavity indeed enhances the non-specific adsorption of hard spheres onto the wall.[13] The critical question here is as follows: Can entropic effect drive the large nucleus to escape from the cell boundary?

The recent theoretical advancement has shown that crowders induced spatial separation between two closed ring-like polymers, a sphero-cylindrical tube due to their entropic effect.[14] A further study investigated the preferential position of a confined polymer chain in a spherical cavity in the presence of crowders. For a semiflexible chain, the polymer is distributed near the cavity boundary because the region allows the chain molecule to avoid crowders and to relieve its bending energy, whereas for a flexible chain, the polymer chain is preferentially distributed in the inner cavity with crowders being blended into the inside of the chain coil.[15]

Recently, Oda *et al.* have conducted an experiment in which a larger granular particle and multiple small ones are confined within a cylindrical cavity, a 2D circular cavity, under vertical vibration.[16] These particles are as rigid as the hard sphere model in liquid state theory. The vertical vibration triggers spatial fluctuations and frequent collisions among particles act like thermal motion in liquid. The experiment was motivated to provide insights into the location of cellular nuclei (or a large organelle). The experimental finding shows that the preferential location of the large particle switches from the region of the cavity wall towards the inner cavity by increasing packing fraction (or crowding level). This result can be roughly

[a)]Electronic mail: chwenyang.shew@csi.cuny.edu

understood based on the mean-field entropic arguments of confined hard spheres. A detailed analysis further reveals that the size disparity between the large particle and small particles is the primary cause. Dynamically, small hard spheres tend to lift the larger hard sphere through their vertical motion, in particular, when the larger sphere is positioned near the cavity wall. While the larger sphere bounces back from the cavity wall at a high enough density of small particles, it may move on the top of small spheres and towards the inner cavity.

To translate the above dynamical behavior into a statistical mechanics understanding on crowding effect, we suggest a simple model to replace the large rigid particle with a soft-boundary sphere. In the near 2D experiment of Oda *et al.*,[16] small particles are able to partially move underneath the larger particle because of their size disparity, similar to partial penetration of smaller particles into the larger particle. This characteristic is consistent with the fact that a nucleus can be viewed as a soft-boundary particle allowing matter exchange across elastic nuclear membranes.[17] By using Monte Carlo simulation, in this work, we intend to investigate the above model for three dimensional crowding systems with aims to identify the possible correlation between the effect of softness of a nucleus (or a large organelle) and its preferential location in a cell under molecular crowding. An integral equation theory is further developed to verify the general structural features observed in our simulation.

II. MODEL AND MONTE CARLO SIMULATION

Here we consider a model that mixes a single large sphere of diameter $D_L = \sigma$ (=$2R_L$) (like the nucleus or a large organelle in a biological cell), which has a soft boundary allowing intrusion on collisions and multiple small hard spheres of diameter D_s (=$2R_s$) as crowders in a 3D rigid spherical cavity of radius R_{cav}. Figure 1 displays the schematic of the model in (a), where D_{Ls} denotes the penetration depth into a large sphere allowed by a small sphere and R_{core} denotes the hard core radius in the soft-boundary large sphere, and the 2D representation of the expected structural feature from the model in (b). Namely, the shortest distance between the hard core of the large sphere and a small sphere can decrease from $R_L + R_s$ (hard sphere limit) to D_{Ls} (soft-boundary large sphere). The (nominal) packing fraction η is defined as $(R_L^3 + N_s R_s^3)/R_{cav}^3$, where N_s is the number of small hard spheres. The cavity size is chosen to be $R_{cav} = 1.1\sigma$ to match that the large particle takes up about 10% of the cavity space as a nucleus in a cell. The interaction potentials between a particle and the cavity wall are given by

$$V(r_i^K) = 0 \quad if \quad r_i^K < R_{cav} - R_K$$
$$= \infty \quad if \quad r_i^K \geq R_{cav} - R_K, \tag{1}$$

where r_i^K is the radial distance of the ith particle of species K measured from the center of the cavity and R_K is the radius of the species K ($R_K = R_L$ and R_s for the large and small sphere, respectively). For the large sphere, this potential defines its outer boundary. The hard core radius inside the large soft-boundary sphere R_{core} is related to the penetration depth D_{Ls},

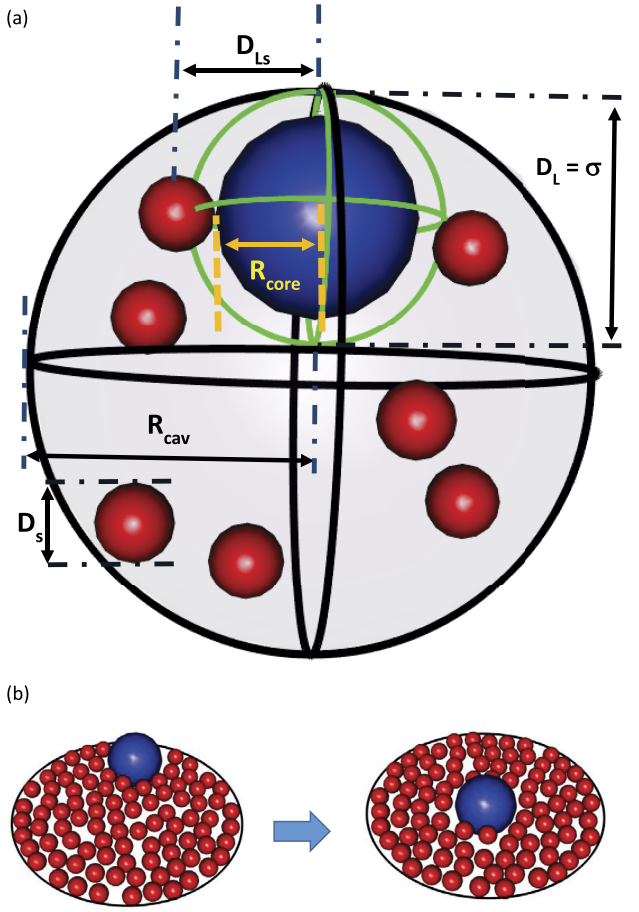

FIG. 1. Plot of schematics of the simulation model in (a), where D_{Ls} denotes the penetration depth into a large sphere allowed by a small hard sphere, D_L (=σ) denotes the diameter of the single large sphere (green spheres), D_s (=$2R_s$) denotes the diameter of N_s small spheres, R_{cav} denotes the cavity radius, R_{core} denotes the hard core radius in the soft-boundary large sphere, and σ is the length unit of this work; the 2D representation of the expected structural feature from the model in (b) in which the large sphere shifts from the periphery (left panel) to inner region (right panel) after the soft boundary is incorporated.

as shown in Fig. 1, and the radius of the crowder R_s (=D_s/2) with the relation given as follows:

$$D_{Ls} = R_{core} + R_s.$$

The interaction potentials between particles are given by

$$V(r_{ij}^{KM}) = 0 \quad if \quad r_{ij}^{KM} < d_{KM}$$
$$= \infty \quad if \quad r_{ij}^{KM} \geq d_{KM}, \tag{2}$$

where r_{ij}^{KM} is the distance between the ith particle of species K and the jth particle of species M measured from their centers and d_{KM} is the minimum distance allowed to approach between a particle from species K particle and a particle from species M. Note that $d_{Ls} = D_{Ls}$ and $d_{ss} = \sigma_s$ in our model that has one large sphere and multiple smaller crowders.

In other words, the large sphere in our model consists of two boundaries: the outer boundary prohibits the large sphere from crossing the cavity wall and the inner boundary is a hard core, like a smaller hard sphere, which cannot be penetrated by smaller crowders. The space between these two boundaries

is empty that can be filled with smaller crowders. This empty space is referred to as "softness" in our model as opposed to the usual hard sphere model with all the space filled up with matters within the sphere.

This empty space inside the large sphere increases the number of ways (or the probability) the crowders around the large sphere in contrast to the case at the hard sphere limit. Qualitatively, this is similar to incorporate attractive interactions between the large sphere and small crowders as a starting point prior to adding the explicit attractive forces into the model. These characteristics act as membranes at the entropic level, that is, allowing matter exchanges and protrusion of cellular matters on membranes.[18] Also, the model captures the entropy effect induced by the multiple ways of interactions between cellular matters and a heterogeneous membrane surface. Figure 1(b) qualitatively depicts the expected structure arising from the model: the large sphere shifts away from the cavity boundary after the soft boundary is incorporated into the large sphere. As the empty space emerges in the large sphere, the small crowders can be driven into this space by osmotic pressure around the large sphere, which can separate the large sphere from the cavity wall.

Monte Carlo simulation is carried out based on the Metropolis algorithm,[19] and the randomly chosen particle undertakes a random walk, in which the displacement of the particle along any given dimension is chosen randomly between $-\delta$ and δ, where δ is the step size. The simulations are tested by three different schemes. First, a particle is randomly picked and is placed in a new position by using the same step size for all species. Second, the step size assigned to the large sphere is different from that assigned to small spheres, and these step sizes are fixed throughout the entire simulation. The step sizes are adjusted in such a way that the acceptance ratio for each species is around 60%. Third, we sample the large particle and small particles with the probabilities 30% and 70%, respectively, to facilitate the large sphere moving around the cavity. In this scheme, we first generate a random number. If this random number is less than 0.3, we attempt a random move for the large sphere; otherwise a small crowder is randomly chosen to perform a random walk. The simulation results are insensitive to the chosen scheme. To calculate the spatial density distribution function for each condition, 2.5×10^9 moves are performed at least, and the first 5×10^8 moves are discarded to assure the system to reach its equilibrium. The simulated density distribution functions and other quantities are obtained by averaging over 10^8 equilibrium configurations.

The primary study here is on the density distribution function of different species, which is defined as follows:

$$\rho_i(r) = \frac{H(r)}{N_T \Delta V(r) N_i}, \tag{3}$$

where i is the large or small sphere; $H(r)$ is the histogram of particles falling into the layer between the radial distance r and $r + \Delta r$ in the simulation, where Δr is the interval of each layer; N_T is the total configurations sampled for calculation; N_i is the number of particles for species i. In the simulation, we divide the cavity into 60 layers and $\Delta r = R_{cav}/60$. The challenge of simulation lies in the volume disparity between periphery and inner cavity, which hinders sufficient sampling around the cavity center.

III. INTEGRAL EQUATION THEORY

We test the features observed in the simulation by using an integral equation theory. As suggested by Zhou and Stell, the integral equation theory for a one-component liquid in a spherical pore can be solved by using Fourier transformation.[20] For the model investigated here, there are three components to be considered including the large sphere, small crowders, and a cavity. The three-component integral equation theory in Fourier k-space (or momentum transfer) takes the following form:

$$\hat{H}_{L3}(k) = \hat{C}_{L3}(k) + \rho_L \hat{H}_{LL}(k)\hat{C}_{L3}(k) + \rho_s \hat{H}_{Ls}(k)\hat{C}_{s3}(k) + \rho_3 \hat{H}_{L3}(k)\hat{C}_{33}(k), \tag{4}$$

$$\hat{H}_{s3}(k) = \hat{C}_{s3}(k) + \rho_L \hat{H}_{sL}(k)\hat{C}_{s3}(k) + \rho_s \hat{H}_{ss}(k)\hat{C}_{s3}(k) + \rho_3 \hat{H}_{s3}(k)\hat{C}_{33}(k), \tag{5}$$

where L, s, and 3 denote the large sphere, small crowders, and the cavity, respectively; ρ_j is the density of the jth species; $\hat{H}_{ij}$ and $\hat{C}_{ij}$ denote the total correlation function and the direct correlation function between i and j species, respectively. Note that the pair correlation function $g_{ij}(r) = h_{ij}(r) + 1$.

Here we consider an isolated cavity, and the above equations are simplified to the following equations by introducing $\rho_3 = 0$ and $\hat{C}_{33} = 0$:

$$\hat{H}_{L3}(k) = \hat{C}_{L3}(k) + \rho_L \hat{H}_{LL}(k)\hat{C}_{L3}(k) + \rho_s \hat{H}_{Ls}(k)\hat{C}_{s3}(k), \tag{6}$$

$$\hat{H}_{s3}(k) = \hat{C}_{s3}(k) + \rho_L \hat{H}_{sL}(k)\hat{C}_{s3}(k) + \rho_s \hat{H}_{ss}(k)\hat{C}_{s3}(k). \tag{7}$$

To incorporate the rigid cavity, we apply the Percus-Yevick (PY) closure to reinforce the hard spherical wall condition, which reads

$$H_{i3}(r) = -1 \quad if\ r > R_{cav}, \tag{8}$$

$$C_{i3}(r) = 0 \quad if\ r \le R_{cav}, \tag{9}$$

where i denotes L or s. As other problems dealing with inhomogeneous fluids in the literature,[22] one possible approximation is to obtain $\hat{H}_{LL}$, $\hat{H}_{Ls}$ (=$\hat{H}_{sL}$), and $\hat{H}_{ss}$ from solving the integral equation of the binary hard sphere mixture in bulk solution. Note that we have compared the results using hypernetted chain and PY closure, and the results for $H_{L3}(r)$ and $H_{s3}(r)$ show little difference in our case. For the soft-boundary large sphere, the minimum distance between the large sphere and a small sphere becomes D_{Ls}.

The fundamental issue to study the liquid structure in a spherical pore is that particle densities are ill-defined and the density distribution function needs to be renormalized as suggested by Kim *et al.*[21] In the integral equation theory, we define the particle density of species i as $\rho_i^0 = N_i/(4\pi R_{cav}^3/3)$, where N_i is the particle number of species i. The density distribution function is calculated as

$$\rho_i(r) = \frac{\rho_i^0 g_{i3}(r)}{\int_0^\infty g_{i3}(r)dr}, \tag{10}$$

where $g_{i3}(r)$ is the pair correlation function species i and 3 (cavity) and is equal to $H_{i3}(r) + 1$. These integral equations

are solved by using the Picard method[22] with 2^9 grids and the interval is 0.01σ. As expected, the numerical theory has limitations and the solution does not converge for small cavities and the crowders of a higher density and/or a smaller size. Nevertheless, we find solutions for crowders of diameter 0.5σ and $R_{cav} \geq 1.5\sigma$. In a slightly larger cavity like $R_{cav} = 2\sigma$, the numerical calculation also converges for crowders of diameter 0.4σ at high enough packing fractions like $\eta = 0.24$. These conditions are sufficient to test the structural features from the present simulation work. Also both theory and simulation considered here are corresponding to the canonical ensemble, and the theory requires no fixed chemical potential as in density functional theory.[21,23]

IV. RESULTS AND DISCUSSION

A. Simulation for the biological cell motivated model

1. Preferential positioning of the soft-boundary large sphere

In the simulation, we first investigate the effect of softness on the structure of the large particle according to its density distribution function under packing fraction $\eta = 0.34$ for small spheres with $D_s = 0.3\sigma$ and the large sphere with $D_L = \sigma$. The cavity size considered here is $R_{cav} = 1.1\sigma$ which is close to a living cell with its nucleus occupying roughly 10% of the entire cell volume. This packing fraction is in the range of cellular crowding. Figure 2 plots the density distribution function of the large particle ρ_L for different penetration depths D_{Ls}, as marked, when $D_s = 0.3\sigma$ in (a), and typical snapshot for $D_{Ls} = 0.6\sigma$ in (b) and 0.65σ in (c), respectively; the predicted histogram of the probability of finding the large particle in the cavity $P(r_i)$ within the ith grid for $D_{Ls}/\sigma = 0.65$ and 0.55 is denoted by solid bars/a solid line and line-pattern bars/a dotted line, respectively, in (d). Note that $P(r_i) = \int_{r_i}^{r_i+\Delta r} 4\pi r^2 \rho_L dr$, where Δr is the grid size of the histogram. The inset in (a) compares three cases of D_{Ls}, as marked, below the hard sphere limit in the semi-log scale. In the case of $D_{Ls} = 0.65\sigma$, the soft boundary of the large sphere diminishes, i.e., the large sphere behaves like a hard sphere. The corresponding density distribution function exhibits the maximum at near the cavity wall, and thus, the large sphere emerges only on the cavity periphery. This result at the hard sphere limit ($D_{Ls} = 0.65\sigma$) is consistent with the picture of the depletion force, suggested by Asakura and Oosawa,[12] in which the preferential location of the confined large object under molecular crowding is next to the cavity wall.

Accompanied by the introduction of softness into the large sphere, the profile of density distribution undergoes a significant change for $D_{Ls} = 0.55\sigma$. The maximum distribution appears close to the center of the cavity along with a smaller peak near $r = 0.38\sigma$. These structure characteristics contradict to the prediction of the depletion force theory. As D_{Ls} is decreased to 0.5σ, the structural features remain similar except that the smaller peak shifts to 0.43σ or so. For $D_{Ls} = 0.45\sigma$, the distribution near the cavity center diminishes pronouncedly. The peak most close to the cavity center now shifts to the position at around $r = 0.18\sigma$, and the other peak near the cavity wall is found at around $r = 0.48\sigma$. By reducing

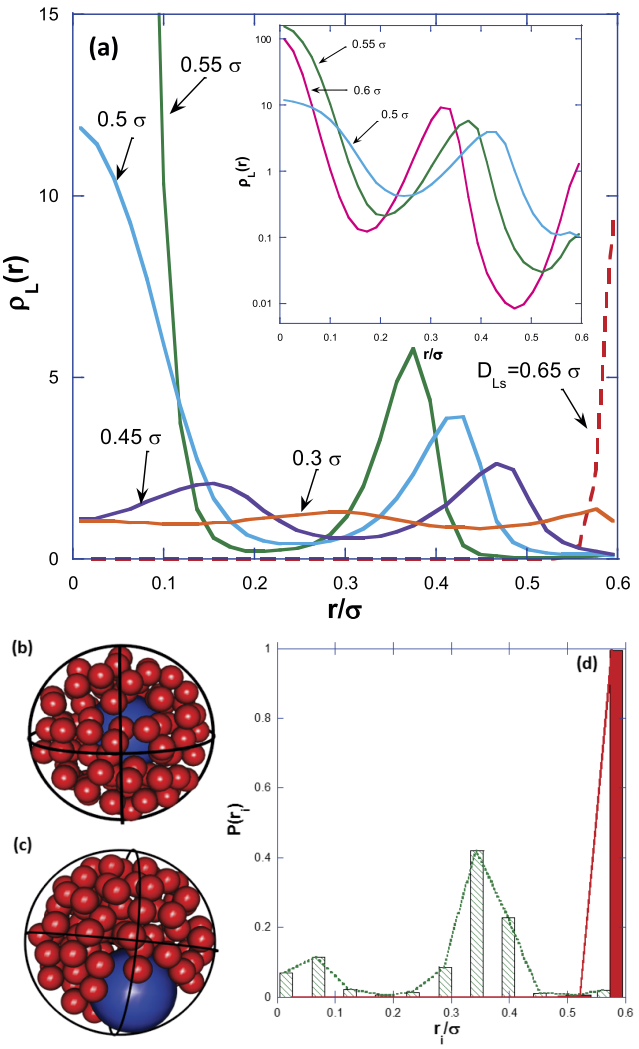

FIG. 2. Plot of the density distribution function of the large particle ρ_L for different penetration depths D_{Ls}, as marked, when $D_s = 0.3\sigma$ in (a); typical snapshots for $D_{Ls} = 0.6\sigma$ in (b) and $D_{Ls} = 0.65\sigma$ in (c), respectively, where $D_{Ls} = 0.65\sigma$ corresponds to the hard sphere limit; the histogram of the probability of finding the large sphere in the cavity $P(r_i)$ within the ith grid for $D_{Ls} = 0.65\sigma$, denoted by solid bars and a line, and 0.55σ, denoted by line-pattern bars and a dotted line (to compare with future experiments) in (d). The inset in (a) is the semi-log plot for greater D_{Ls}, as marked. The lines in (d) are a guide to the eye.

D_{Ls} to 0.3σ, the density distribution function becomes quite flat in the whole range of r. In the inset of Fig. 2(a), centralization of the soft-boundary large sphere at around the cavity center is observed for three different cases of D_{Ls}. The density distribution function of $D_{Ls} = 0.60\sigma$ manifests the weak attachment of the large sphere to the cavity wall compared to that of $D_{Ls} = 0.65\sigma$.

At near the cavity center ($r = 0$), we find the peak of global maximum for $D_{Ls} = 0.60\sigma$, indicating that centralization of the soft-boundary large hard sphere becomes a key process to establish its structure. As D_{Ls} is decreased from 0.60σ to 0.55σ, a significant decrease in the distribution of the soft-boundary large sphere near the cavity boundary is observed, and the centralization process is greatly enhanced. The snapshots in Figs. 2(b) and 2(c) illustrate this finding, in which the large sphere shifts its preferential positioning to the inner cavity [Fig. 2(b) for $D_{Ls} = 0.6\sigma$] from the

TABLE I. Position of the peak near cavity wall for $\eta = 0.34$ and $R_s = 0.15\sigma$.

D_{Ls}/σ	Approximate position from simulation (in σ)	$(R_{cav} - D_{Ls} - R_s)/\sigma$
0.60	0.32	0.35
0.55	0.38	0.40
0.50	0.43	0.45
0.45	0.48	0.50

location near the cavity boundary proximity [Fig. 2(c)] at the hard sphere limit with $D_{Ls} = 0.65\sigma$. By decreasing D_{Ls} from 0.55σ to 0.50σ, the centralization process is weakened along with a decrease of the density distribution function at near $r = 0$. The histogram of ρ_L in Fig. 2(d) shows the probability of finding the large sphere in the cavity predicted by the model to compare with the future experimental observation similar to the work by Oda *et al.*[16] It predicts that the large sphere with the soft boundary tends to distribute in inner cavity more frequently but the rigid large sphere distributes around periphery.

The important structural features in Fig. 2 are summarized as follows. For D_{Ls}/σ in the range between 0.60 and 0.45, the density distribution function from simulation displays two main peaks: one is near the cavity wall (not next to the wall) and the other is near the cavity center. The dependence of the position for the peak near the cavity wall on D_{Ls} is summarized in Table I. The simulated peak position is roughly comparable with the equation $R_{cav} - D_{Ls} - R_s$. Besides, it is noticeable that in Fig. 2 the density distribution near $r = 0$ decreases significantly when D_{Ls}/σ is varied from 0.50 to 0.45. While D_{Ls}/σ is decreased from 0.45 to 0.30, the soft-boundary large sphere (in inner cavity) behaves more like a crowder. All these findings will be discussed further below.

In the hard sphere limit, the large sphere tends to attach onto the cavity wall due to the depletion force with the cavity wall under the crowding level being studied here. The softness induces "desorption" of the large sphere from the wall as illustrated in the schematics of Fig. 3. The figure exhibits two possible pictures arising from the excluded volume interactions among the small spheres, the cavity wall, and the soft-boundary large sphere. Figure 3(a) shows the case of $R_L - R_s < D_{Ls} < R_L + R_s$, and Fig. 3(b) is for $D_{Ls} \le R_L - R_s$. The "transverse" depletion force is due to packing of small crowders against the contact area of the outermost surface of the large sphere and the cavity boundary, and the "radial" depletion force is originated from the packing of the large sphere against the cavity boundary due to smaller crowders. The reason that the large sphere escapes from the cavity boundary occurring for $R_L - R_s < D_{Ls} < R_L + R_s$ is attributed to the free space generated by the "soft" interior of the large sphere. Note that a small hard sphere is allowed to penetrate into the large sphere up to the distance D_{Ls}. Below this distance is the forbidden region in which the small sphere unphysically overlaps with the hard core inside the large sphere.

At a high enough packing fraction, a greater number of small spheres distributes around the cavity wall. With the soft-boundary large sphere next to the cavity boundary, it creates an exclusion zone that cannot be accessed by any small particles, which causes a greater osmotic pressure, as the solid arrows and shaded area shown in the right panel of Fig. 3(a). In contrast, when the soft-boundary large sphere becomes distant from the cavity wall, small spheres pack themselves onto the cavity wall as well as the surface of the hard core inside the soft-boundary large sphere to increase the interior free volume of the cavity, a mechanism to relieve the osmotic pressure. Namely, the "transverse" depletion force (solid arrows) is more advantageous than the "radial" depletion force (open arrows) in Fig. 3(a). As a result, the soft-boundary large sphere tends to shift away from the regime close to the cavity wall. As seen in the inset of Fig. 2, by incorporating the soft boundary, the large sphere starts to escape from the cavity wall for $D_{Ls} = 0.60\sigma$ and to increase its presence at the cavity center. A further decrease of D_{Ls} to 0.55σ enhances this scenario. The preferential position of the soft-boundary large sphere, which is most close to the cavity boundary (not next to the wall), occurs at near $R_{cav} - D_{Ls} - R_s$, consistent with the simulation result for those cases summarized in Table I. Note that spatial fluctuation may contribute to the minor difference between simulation and theoretical prediction.

For D_{Ls} smaller than $R_L - R_s$, the space between R_L and the hard core inside the soft-boundary large sphere allows small hard spheres to bypass the hard core area when the soft-boundary large sphere is next to the cavity wall as shown in the schematic of Fig. 3(b). The "transverse" depletion force dominates because the "radial" depletion force has no significant

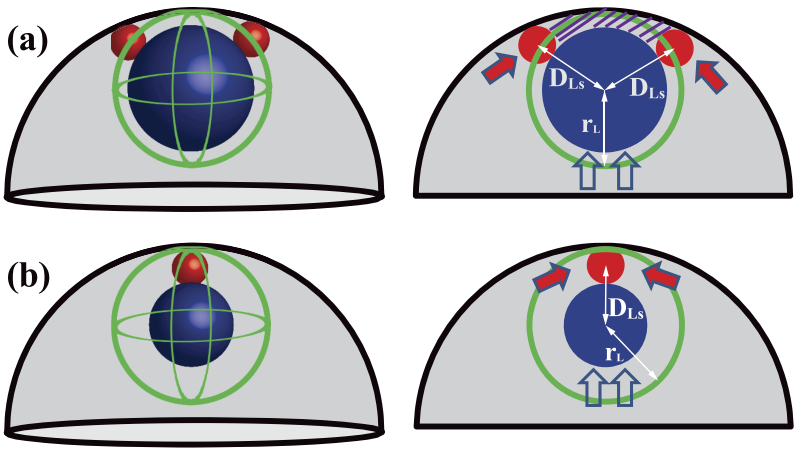

FIG. 3. Schematic plot of two possible pictures arising from the excluded volume interactions among the small spheres of radius R_s, the cavity wall and the soft-boundary large sphere of radius R_L for the case $R_L - R_s < D_{Ls} < R_L + R_s$ in (a) and $D_{Ls} \le R_L - R_s$. in (b). The left panels are 3D schematics and the right panels display their vertical cross-sectional view. The shaded area in the right schematic of Fig. 3(a) denotes the exclusion zone for small spheres due to the soft-boundary large sphere at near the cavity wall. The solid arrows and the open arrows denote the likely "transverse" and "radial" depletion forces, respectively, explained in the context of the figure.

contribution (no contact between the hard core of the large sphere and the cavity wall). Meanwhile the free space in the cavity increases due to the shrinkage of the hard core of the soft-boundary large sphere. Hence, the effect of the hard core of the soft-boundary large sphere becomes secondary as in the case of $D_{Ls} = 0.30\sigma$ ($<R_L - R_s$) in Fig. 2. Note that when $R_L = 0.50\sigma$ and $R_s = 0.15\sigma$, we have $R_L - R_s = 0.35\sigma$. The most significant finding in these studies is that the soft boundary of the large sphere triggers the large sphere to escape from the cavity wall. Such a finding is consistent with the common picture that the preferential location of a large organelle is away from the region of periphery.

2. Structure of smaller crowders in a cavity

The preferential location of the soft-boundary large sphere has a direct impact on the spatial distribution of small hard spheres. Figure 4 plots the density distribution function of small hard spheres of $D_s = 0.3\sigma$ for different D_{Ls}'s, as marked, and the 2D representations to explain the different structure between a larger (left panel) and a smaller (right panel) D_{Ls} in (b). When the large sphere is in its hard sphere limit ($D_{Ls} = 0.65\sigma$), the density distribution of small spheres in Fig. 4(a) shows liquid-like ordering with the maximum found around the cavity wall. At the area very close to $r = 0$, the probability

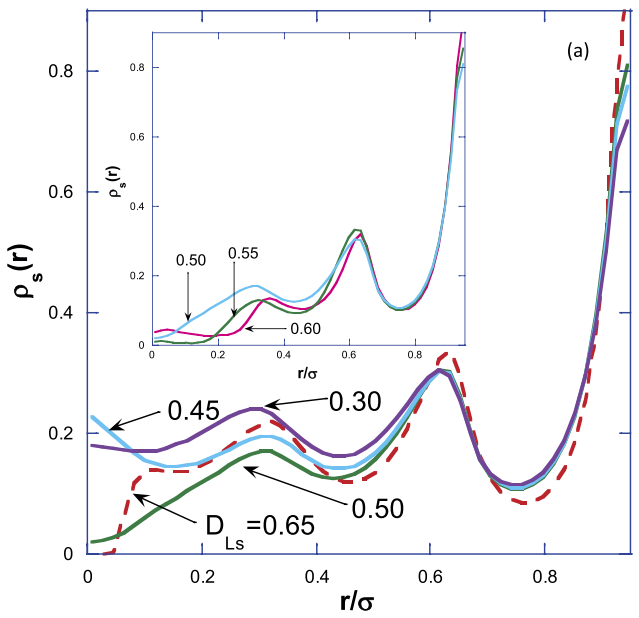

FIG. 4. Plot of the density distribution function of small spheres ρ_s in (a), including the inset, for different D_{Ls}'s, as marked, when $D_s = 0.3\sigma$ (same parameters as in Fig. 2); the 2D representations to account for the different structure between a larger (left panel) and a smaller (right panel) D_{Ls} in (b).

of finding small particles quickly drops to zero because the size of the large sphere blocks a smaller crowder of size $D_s = 0.3\sigma$ to access the cavity center. For $D_{Ls} = 0.50\sigma$, its ρ_s decreases continuously from $r = 0.3\sigma$ towards $r = 0$. At $r = 0$, ρ_s remains low but becomes non-zero. This feature is more like the correlation hole caused by repulsive forces[24] which are originated from the hard core of the soft-boundary large sphere in this case. Similar cases are shown in the inset of Fig. 3(a) for greater D_{Ls}. When $D_{Ls} = 0.45\sigma$, the region of the correlation hole disappears, indicating that small spheres tend to move more freely in this region. A further discussion on this finding will be given next.

For a large enough D_{Ls} ($\geq 0.50\sigma$), the soft-boundary large sphere exhibits a higher tendency to distribute at near the center of the cavity. This centralization process attenuates as D_{Ls} is decreased to $D_{Ls} = 0.45\sigma$, for instance. The possible physical origin can be understood as follows. After the large sphere of a larger D_{Ls} drifts away from periphery, tight packing of small spheres onto the surface of the hard core of the large sphere creates an entropically favorable process to increase the free volume inside the cavity as shown in the left schematic of Fig. 4(b). By placing the soft-boundary large sphere at the center of the cavity, small crowders can have a more equal distribution at all directions, which favors the system entropy. The decrease of D_{Ls} from $D_{Ls} = 0.50\sigma$ to 0.45σ may trigger the following two mechanisms for smaller crowders as shown in the right 2D schematic of Fig. 4(b): (1) the free volume of the cavity is increased and (2) the hard core surface of the soft-boundary large sphere is decreased. Since the particle density around the hard core of the soft-boundary large sphere is roughly scaled as $1/D_{Ls}$ (the number of crowders adsorbed onto the hard core surface of the large sphere $\sim D_{Ls}^2$ and the volume occupied by the adsorbed spheres $\sim D_{Ls}^3$). Therefore, the smaller D_{Ls} (for example, $D_{Ls} = 0.45\sigma$) induces a greater particle density of smaller crowders around the hard core of the soft-boundary large sphere, causing a greater local osmotic pressure[25] and diffusivity (concentration gradient),[26] both of which drive the large sphere (attached with small crowders) to the lower density region. Consequently, for $D_{Ls} = 0.45\sigma$, the soft-boundary large sphere moves away from the cavity center, and the peak (most close to the cavity center) is now at around $r = 0.15\sigma$ in Fig. 2, illustrated in the right schematic of Fig. 4(b). As a matter of fact, this peak position (in ρ_L) is actually near a local minimum of ρ_s in Fig. 3, an area that has a lower local crowder density.

3. Effect of crowder size

The excluded volume interaction between small hard spheres and the soft-boundary large sphere is an essential factor to induce migration of the large sphere away from the cavity wall. It is instructive to reveal the role of the steric hindrance of small spheres on this issue by changing the size of small spheres but keeping the crowding level intact. In the following are the simulation results to investigate the structural property of the large sphere when the diameter of small spheres is decreased from 0.30σ to 0.2σ but keeping the packing fraction η at 0.34 same as in Fig. 2 (in the range of cellular crowding). Figure 5 plots the density distribution function of the large sphere for different D_{Ls}'s, as marked, when $D_s = 0.2\sigma$ in (a),

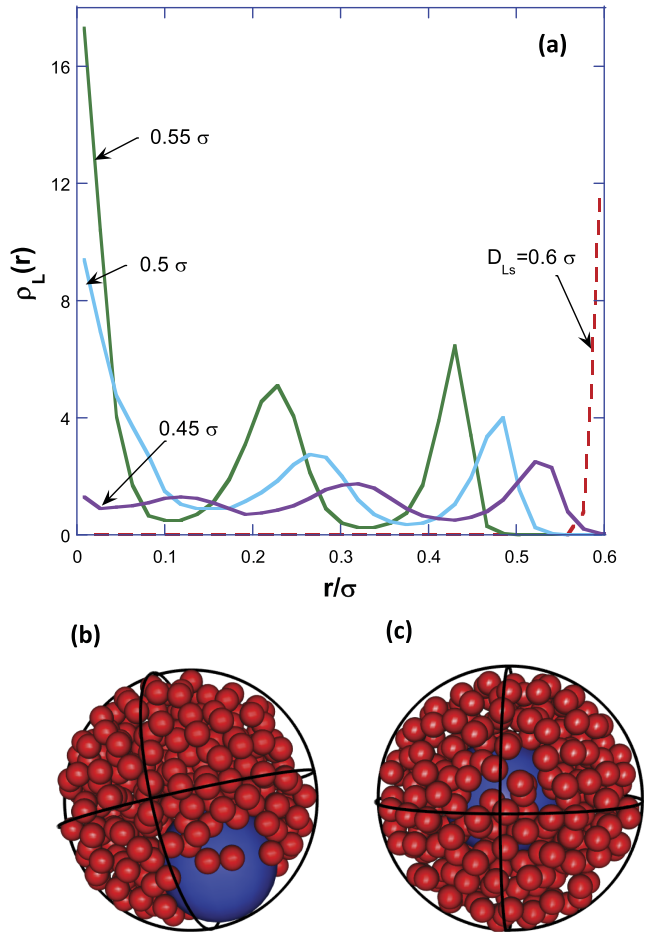

FIG. 5. Plot of the density distribution function of the large sphere for different D_{Ls}'s, as marked, when $D_s = 0.2\sigma$ (different from Fig. 2) in (a); typical snapshots for $D_{Ls} = 0.6\sigma$ in (b) and $D_{Ls} = 0.55\sigma$ in (c), respectively, where $D_{Ls} = 0.6\sigma$ corresponds to the hard sphere limit.

and the typical snapshots for $D_{Ls} = 0.6\sigma$ in (b) and 0.55σ in (c). When $D_s = 0.20\sigma$, the parameter $D_{Ls} = 0.60\sigma$ corresponds to the hard sphere limit. As expected, the large sphere tends to attach to the cavity wall. After the soft boundary is incorporated into the large sphere, i.e., for those $D_{Ls} < 0.60\sigma$ in the figure, the large sphere distributes away from the cavity wall. These observations are consistent with the snapshots shown in Figs. 5(b) and 5(c). In each case, the density distribution function has multiple peaks arising form the competition of spatial packing with small spheres.[18] The peak most close to the cavity wall follows the similar pattern as in Table I, and the position is roughly equal to $R_{cav} - D_{Ls} - R_s$.

For large enough D_{Ls} like 0.55σ and 0.5σ, centralization of the soft-boundary large sphere at the cavity center can be observed. The corresponding density distribution functions at $r = 0$ are not as prominent as those in Fig. 2(a). This result suggests that reducing the size of smaller crowders may offset the centralization process of the soft-boundary large sphere but does not compromise the fact that the soft boundary is essential to facilitate the large sphere to escape from the cavity wall. Moreover, as D_{Ls} is decreased to 0.45σ in Fig. 5(a), the cavity gains enough free volume and centralization of the soft-boundary large sphere at $r = 0$ becomes less pronounced. Nevertheless, escape of the soft-boundary large sphere away from the cavity wall can be clearly observed along with a greater probability for the large sphere to be found in the cavity interior than in the region next to the cavity wall. Such a trend of specific localization found in the present study is relevant to the cellular materials that contribute to molecular crowding, and the crowders in a cell may have a sufficiently large size through aggregation of cellular biopolymers to sustain the centralization process of a nucleus or a large organelle in a cell.

Despite the fact that the 3-D model is considered here, the predictions arising from this model are quite general, which generate similar features observed in the previous vibration experiment done by Oda *et al.*[16] The work by Oda *et al.* investigated a mixture consisting of a larger granular particle and multiple smaller granular particles confined within a 2D circular disk under vertical vibration. The vibration motion of particles induced frequent collisions among them, and the system can be viewed as a quasi-2D hard sphere mixture. Due to the size disparity, the smaller spheres are allowed to move into the space under the larger sphere. Two important findings were reported: the preferential location of the larger particle shifts from the region near the cavity wall to the inner cavity by (1) decreasing the size of the smaller particles at a high enough particle density and (2) increasing the density of smaller particles of a given crowder size. Figure 6 plots ρ_L for $D_s = 0.3\sigma$ and 0.2σ for different D_{Ls}'s, as marked, when $\eta = 0.34$. In the hard sphere limit, ρ_L at the cavity wall (near $r = 0.6\sigma$) is increased by decreasing D_s from 0.3σ to 0.2σ, indicating that smaller crowders are more effective to maintain the depletion force between the larger sphere and the cavity wall.[30] While the value of D_{Ls} is reduced by 0.05σ compared to the corresponding hard sphere limit for each D_s, the result shows that

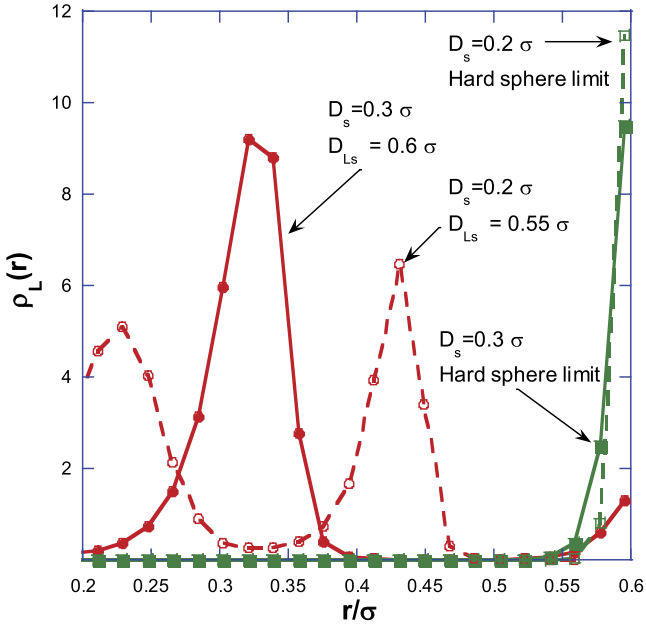

FIG. 6. Plot of the density distribution function of the large sphere ρ_L for $D_s = 0.3\sigma$ and 0.2σ for different D_{Ls}'s, as marked, when $\eta = 0.34$. Symbols denote simulation results to clarify parameters in calculation, and the lines are a guide to the eye. The hard sphere limits have the same parameters as those in Fig. 2 ($D_{Ls} = 0.65\sigma$ for $D_s = 0.3\sigma$) and this figure ($D_{Ls} = 0.6\sigma$ for $D_s = 0.2\sigma$).

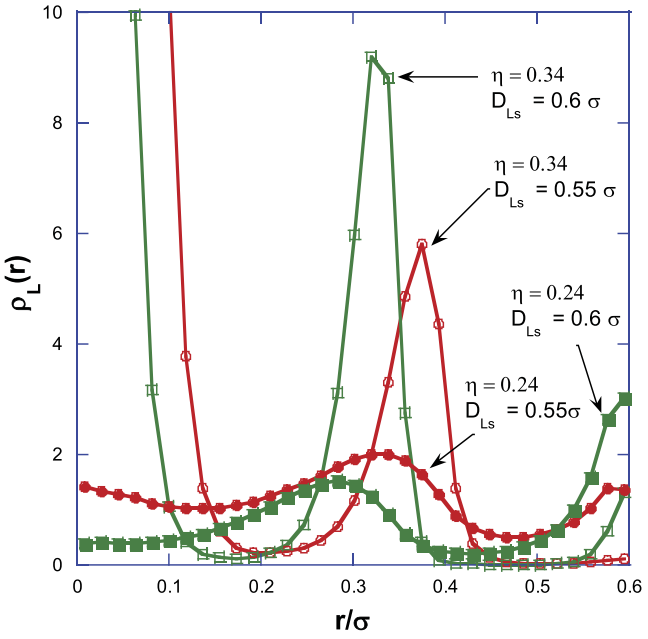

FIG. 7. Plot of ρ_L for the packing fraction $\eta = 0.24$, denoted by solid symbols, and 0.34, denoted by open symbols, for $D_{Ls} = 0.55\sigma$, denoted by circles, and 0.6σ, denoted by squares when $D_s = 0.3\sigma$. Symbols denote simulation results to clarify parameters in calculation, and the lines are a guide to the eye.

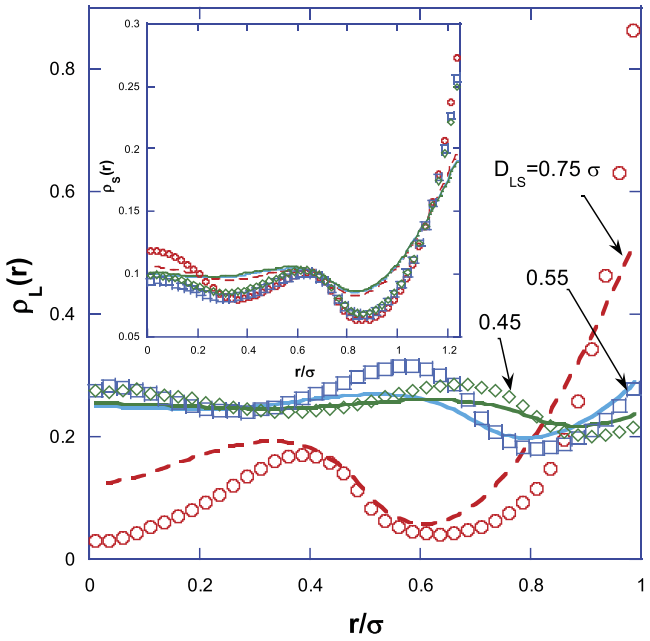

FIG. 8. Comparison of ρ_L from simulation, denoted by symbols, and theory, denoted by lines, for different D_{Ls}'s as marked when $\eta = 0.189$, $R_{cav} = 1.5\sigma$, and $R_s = 0.5\sigma$. Note that the dotted line denotes the hard sphere limit when $D_{Ls} = R_L + R_s$. The inset is the same plot but for ρ_s.

the smaller crowder size D_s (=0.2σ) enhances migration of the soft-boundary large sphere into the inner cavity (away from the cavity wall), whereas the soft-boundary large sphere under the crowders with the greater D_s (=$0.3\ \sigma$) exhibits the perceivable probability to adhere to the cavity wall.

Figure 7 plots ρ_L for the packing fraction $\eta = 0.24$, denoted by solid symbols, and 0.34, denoted by open symbols, for $D_{Ls} = 0.55\sigma$, denoted by circles, and 0.6σ, denoted by squares when $D_s = 0.3\sigma$. The D_{Ls} values chosen here are corresponding to the soft-boundary large sphere. At the lower packing fraction $\eta = 0.24$, the large sphere for both cases $D_{Ls} = 0.55\sigma$ and 0.6σ has displayed a higher probability to be located near the cavity wall because the number of crowders that occupies the region near the cavity wall is expected to be smaller than that of $\eta = 0.34$. As a result, the forbidden zone near the wall created by the soft-boundary large sphere, as shown in Fig. 3(a), becomes less essential for small spheres along with the weaker "transverse" force. Since the "radial" depletion remains significant, ρ_L near the cavity wall with smaller η (=0.24) in Fig. 7 is greater for both D_{Ls} compared to their counterparts for $\eta = 0.34$. Such a result suggests that a higher packing fraction facilitates the soft-boundary large sphere shifting to the inner cavity. It is instructive to point out that the findings of Figs. 6 and 7 are consistent with the experimental observations in the previous work by Oda *et al.*,[16] but the current work provides physical insights into the experimental findings.

B. Testing simulation results with theory

1. Dependence of the softness of the soft-boundary large sphere on structure

To test the above predictions of the model, we compare the results of integral equation theory with those of simulation. Figure 8 displays ρ_L for various D_{Ls}, as marked, when $\eta = 0.189$, $R_{cav} = 1.5\sigma$, and $R_s = 0.5\sigma$. The inset is the same plot except for ρ_s. The theory predicts similar features as shown in the simulation. At the hard sphere limit (dashed line in Fig. 8), ρ_L exhibits the maximum at near the cavity wall ($r = R_{cav} - 0.5\sigma$). Since the packing fraction is low, the second peak emerges at near $r/\sigma = 0.38$ in theory, similar to the simulation result. As D_{Ls} is decreased, the peak near the cavity wall diminishes, and the large sphere shifts to the cavity interior. The highest peak moves closer to the inner cavity when D_{Ls} is decreased from 0.55 to 0.45. The results of theory show qualitative agreement with simulation, and such behavior is consistent with the results summarized in Table I. For crowders at this packing fraction, ρ_s shows little change among three different D_{Ls}'s due to the lower packing fraction and larger cavity size. A minor difference is found in both simulation and theory in which for $D_{Ls} = 0.75\sigma$, the smaller sphere has a slightly greater chance to be near at the cavity center, a feature not seen in Fig. 4, which can be attributed to the larger cavity size here. Quantitatively, the theory underestimates the contact value around the cavity boundary and overestimates the density distribution in the inner cavity. Nonetheless, the theory predicts the essential features seen in our simulation results.

2. Packing fraction effect on the preferential positioning of the soft-boundary large sphere

Figure 9 compares ρ_L from simulation (symbols) and from theory (lines) for two different packing fractions $\eta = 0.28$ (solid symbols and solid lines) and 0.189 (open symbols and dashed lines) with $D_{Ls}/\sigma = 0.55$ and 0.45, as marked, when $R_{cav} = 2\sigma$ and $R_s = 0.25\sigma$. Both theory and simulation show reasonable agreement for the soft-boundary large sphere at the two densities. For the greater D_{Ls}/σ (=0.55), ρ_L next to the wall diminishes more significantly for the greater packing

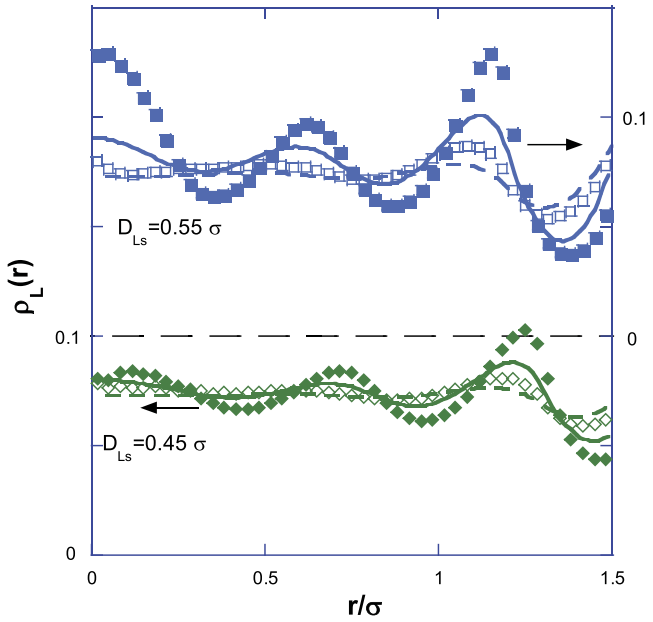

FIG. 9. Plot of ρ_L from simulation, denoted by symbols, and from theory, denoted by lines for $\eta = 0.28$ (solid symbols and solid lines) and 0.189 (open symbols and dashed lines) with $D_{Ls} = 0.55\sigma$ and 0.45σ, as marked, when $R_{cav} = 2\sigma$ and $R_s = 0.25\sigma$. The y-axes for $D_{Ls}/\sigma = 0.55$ and 0.45 are on right and left, respectively, as indicated by the direction of the arrows.

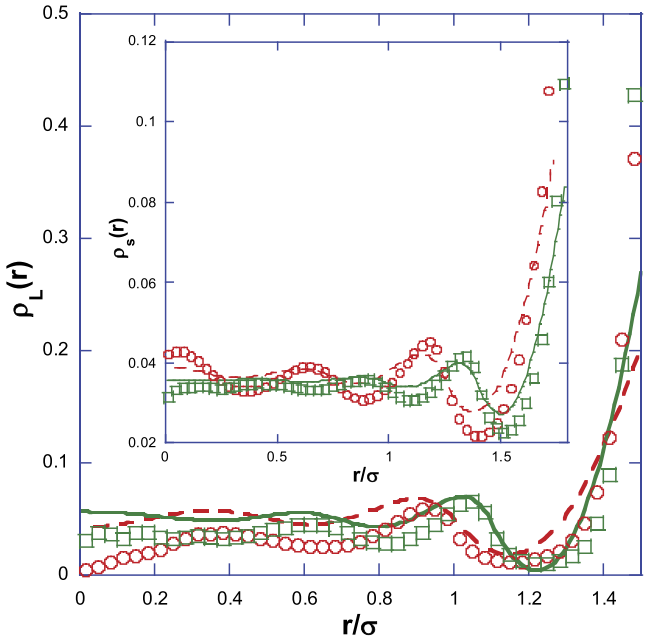

FIG. 10. Plot of ρ_L between simulation, denoted by symbols, and theory, denoted by lines at the hard sphere limit for $R_s/\sigma = 0.25$, denoted by open circles and solid line, and 0.2, denoted by open squares and dashed line, when $\eta = 0.24$ ($D_{Ls}/\sigma = 0.75$ and 0.7 for $R_s/\sigma = 0.25$ and 0.2, respectively). The inset is the same plot except for ρ_s.

fraction together with a more pronounced oscillatory pattern. While D_{Ls} is reduced to 0.45σ, ρ_L is enhanced at near the cavity boundary, but the oscillatory structure in ρ_L becomes less marked. The peaks in the inner cavity and near the wall (not next to the wall) for both D_{Ls} follow the spatial packing pattern similar to Table I. At the cavity center $r = 0$ for $D_{Ls} = 0.55\sigma$, the tighter spatial packing among particles under a greater η (=0.28) induces a higher density distribution. Once D_{Ls} is lowered to 0.45σ, the density distribution near $r = 0$ decreases. All of the above trends are similar to those shown in Fig. 7.

3. Crowder sizes and the structure of confined particles

To test the size effects of crowders, Fig. 10 compares ρ_L between $R_s/\sigma = 0.25$, denoted by squares (simulation) and solid lines (theory), and $R_s/\sigma = 0.2$, denoted by circles (simulation) and dotted lines (theory) at the hard sphere limit when $\eta = 0.24$ and $R_{cav}/\sigma = 2$. Note that $D_{Ls}/\sigma = 0.75$ and 0.7 for $R_s/\sigma = 0.25$ and 0.2, respectively, in this limit. The inset is the same plot except for ρ_s. For ρ_L, the contact value of the large sphere near the wall rises more by mixing with crowders of a smaller size (i.e., $R_s/\sigma = 0.2$), similar to Fig. 6. For crowders, both $R_s/\sigma = 0.25$ and 0.2 display an oscillatory pattern, but the oscillation is more marked for the larger crowders. At near $r = 0$, the oscillatory structure remains in ρ_s for larger crowders, whereas ρ_s of smaller crowders become flattened. These findings indicate that the larger crowders pack more tightly and the smaller crowders experience more spatial fluctuation.

We further compare the simulation and theory for ρ_L of the soft boundary large sphere in Fig. 11 that is the same plot as in Fig. 10 except that D_{Ls}/σ is changed to 0.55 and 0.5 for $R_s/\sigma = 0.25$ and 0.2, respectively. In both cases of Fig. 11, ρ_L near the wall is lower than those in Fig. 10. The multiple peaks in the layer structure of ρ_L shift to smaller r as R_s is decreased. Qualitatively, a similar behavior has been found in Fig. 6.

In the range of conditions that we find solutions for the integral equation theory, the theoretical predictions are in reasonable agreement with the simulation results. The theory renders an opportunity to verify our simulation work for the much smaller cavity that has biological implications.

The introduction of softness into the large sphere seems to lessen the crowding level of the system, but its effect is quite

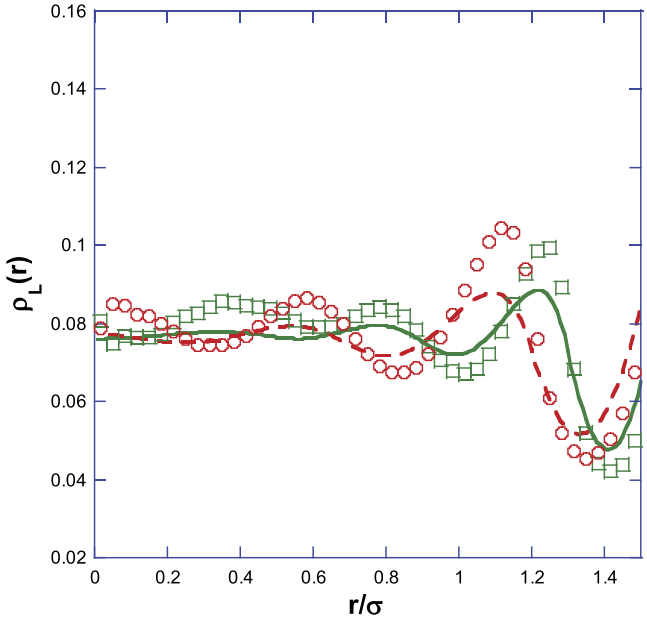

FIG. 11. Same plot of ρ_L as Fig. 10 except that the large sphere has a soft boundary with $D_{Ls}/\sigma = 0.55$ and 0.5 for $R_s/\sigma = 0.25$ and 0.2, respectively.

different from gaining free volume by decreasing the density of small spheres. These two processes are likely to occur in different length scales. As in the past study, we have made it clear that a decrease of crowding level by lowering the number of crowders causes the localization of the large sphere adjacent to the cavity boundary (other than driving its localization in the inner cavity).[16] Such an opposite trend suggests the scientific importance of this topic on the further study, i.e., it is highly expected that the localization of the large sphere is critically dependent on the manner of interaction with the crowders. In other words, a change in the detailed interaction potential would play a significant role on the specific localization.

V. CONCLUSIONS

The large organelle like the nucleus of eukaryotic cells is commonly observed in the region away from the cellular membrane, including the center of the cavity. Since the interior of a cell is highly crowded, excluded volume interactions are essential to elucidate the preferential location of the nucleus. To better understand this problem from the standpoint of entropy, we investigate a simple athermal model consisting of a soft-boundary large hard sphere and small hard spheres as crowders by using the Monte Carlo simulation and an integral equation theory. In the range that the theory has solutions, both simulation and theory are in reasonable agreement qualitatively. We find that the soft boundary of the larger particle allows small hard spheres to partially penetrate into the large sphere, which causes the larger sphere to escape from the cavity wall. The result is consistent with the general view regarding the preferential location of the large organelle like the nucleus in a biological cell. This finding is not surprising because large organelles like nuclei have soft boundaries by nature, which allows matter exchange in-and-out the elastic nuclear membrane. As a matter of fact, such a trend is different from the usual depletion force argument that the larger sphere is expected to attach to the cavity wall under molecular crowding. Besides, for the large enough small spheres as crowders, the moderate penetration depth into the large sphere may facilitate centralization of the large particle away from the cavity boundary including the central region of the cavity at the level of cellular crowding. Considering the cytoplasm materials in a cell, we may find multiple large crowders originating from cellular organelles and aggregates of biomacromolecules to facilitate centralization of nuclei within the cell. From the model study in this work, we conclude that entropic effect alone can serve as a driving force for the escape of the nucleus away from cellular membrane by its soft boundary.[27]

Besides, we find that the 3D model considered in this work provides the essential physical insights into the quasi-2D vibration experiment by Oda *et al.*[16] Furthermore, the simple model may account for the physical origin of the centralization of DNA in prokaryotic cells without nuclear membranes.[28] In this case, one may treat the contract DNA in a prokaryotic cell as a porous sphere that allows matter exchange, and at the level of our model, centralization of DNA is expected under molecular crowding. Also, considering a flexible chain confined in a crowded spherical cavity, our model may explain the simulation results by Shin *et al.*[15] If we view the chain coil as a soft-boundary sphere allowing crowders to penetrate it, the polymer chain may find its preferential position in the inner cavity as shown in their work.[15] Our future work will be focused on how the detailed interactions between the larger particle and crowders may impact the preferential location of the larger particle like the cellular nucleus. Meanwhile we will test the possibility to further extend the integral equation to investigate the condition more close to the length scale and the complexity of a biological cell. Most importantly, the boundary where the large sphere starts to migrate from the cavity periphery into the inner cavity will be elucidated by integrating the current work with the mean field theories from our previous studies in characterizing such a boundary.[16,29] The boundary can be a complicated function with crowder size, crowder density, cavity size, etc., which will provide insights into the nature of transition.

ACKNOWLEDGMENTS

C.-Y.S. thanks the partial support from the City University of New York PSC Grant (Nos. 67134-0045 and 68108-0046) and from the JSPS Invitation Award (No. S12033). S.O. thanks the partial support from the Sasakawa Scientific Research Grant (No. 28-229) from The Japan Science Society. K.Y. thanks the partial support from JSPS KAKENHI Grant Nos. 15H02121 and 25103012.

[1] S. B. Zimmerman and A. P. Minton, Annu. Rev. Biophys. Biomol. Struct. **22**, 27 (1993).
[2] R. J. Ellis, Curr. Opin. Struct. Biol. **11**, 114 (2001).
[3] H. Lodish, A. Berk, P. Matsudaira, C. A. Kaiser, M. Kriege, M. P. Scott, S. L. Zipursky, and J. Darnell, *Molecular Cell Biology*, 5th ed. (W. H. Freeman, New York, 2004).
[4] *Molecular Biology of the Cell*, 4th ed., edited by B. Alberts, A. Johnson, J. Lewis, M. Raff, K. Roberts, and P. Walter (Garland Science, 2002), Chap. 4, pp. 191–234.
[5] V. A. Chepurnov, D. G. Mann, W. Vyverman, and K. Sabbe, J. Phycol. **38**, 1004 (2002).
[6] Y. Desfougeres, H. Neumann, and A. Mayer, J. Cell Sci. **129**, 2817 (2016).
[7] H. N. Anna, A. H. N. Griffis, N. R. Groves, X. Zhou, and I. Meier, Front. Plant Sci. **5**, 129 (2014).
[8] K. Richter, M. Nessling, and P. Lichter, Biochim. Biophys. Acta **1783**, 2100–2107 (2008).
[9] P. H. Raven, G. B. Johnson, K. A. Mason, J. Losos, and S. Singer, *Biology*, 11th ed. (McGraw-Hill Education, New York, 2016).
[10] K. Yoshikawa, S. Hirota, N. Makita, and Y. Yoshikawa, J. Phys. Chem. Lett. **1**, 1763 (2010).
[11] N. A. Denesyuk and D. Thirumalai, J. Phys. Chem. B **5**, 225 (2013).
[12] S. Asakura and F. Oosawa, J. Chem. Phys. **22**, 1255 (1954).
[13] R. Roth, B. Götzelmann, and S. Dietrich, Phys. Rev. Lett. **83**, 448 (1999).
[14] J. Shin, A. G. Cherstvy, and R. Metzler, New J. Phys. **16**, 053047 (2014).
[15] J. Shin, A. G. Cherstvy, and R. Metzler, ACS Macro Lett. **4**, 202 (2015).
[16] S. Oda, Y. Kubo, C.-Y. Shew, and K. Yoshikawa, Physica D **336**, 39 (2016).
[17] E. Lindahl and O. Edholm, Biophys. J. **79**, 426 (2000).
[18] C.-Y. Shew, K. Kondo, and K. Yoshikawa, J. Chem. Phys. **140**, 024907 (2014).
[19] N. Metropolis, A. W. Rosenbluth, M. N. Rosenbluth, A. H. Teller, and E. Teller, J. Chem. Phys. **21**, 1087 (1953).
[20] Y. Zhou and G. Stell, Mol. Phys. **66**, 767 (1989).
[21] S.-C. Kim, S.-H. Suh, and C. H. Lee, J. Korean Phys. Soc. **35**, 350 (1999).

[22]J.-P. Hansen and I. R. McDonald, *Theory of Simple Liquids*, 2nd ed. (Academic Press, New York, 1990).
[23]A. Gonzalez, J. A. White, F. L. Roman, and S. Velasco, Phys. Rev. Lett. **79**, 2466 (1997).
[24]K. S. Schweizer and J. G. Curro, Adv. Polym. Sci. **116**, 321 (1994).
[25]M. Kinoshita, Biophys. Rev. **5**, 283 (2013).
[26]A. Zaccone and E. M. Terentjev, Phys. Rev. E **85**, 061202 (2012).
[27]E. Sackmann, "Physical basis of self-organization and function of membranes: Physics of vesicles," in *Handbook of Biological Physics* (Elsevier, 1995), Vol. 1, pp. 213–303.
[28]M. Joyeux, J. Phys. Chem. B **121**, 6351 (2017).
[29]C.-Y. Shew and K. Yoshikawa, Chem. Phys. Lett. **590**, 196 (2013).
[30]X. L. Chu, A. D. Nikolov, and D. T. Wasan, Langmuir **12**, 5004 (1996).